ChemComm

RSC Publishing

COMMUNICATION

View Article Online
View Journal | View Issue

SnO_2@graphene nanocomposites as anode materials for Na-ion batteries with superior electrochemical performance†

Cite this: *Chem. Commun.*, 2013, **49**, 3131

Received 18th January 2013,
Accepted 27th February 2013

DOI: 10.1039/c3cc40448j

www.rsc.org/chemcomm

Dawei Su,[a] Hyo-Jun Ahn[b] and Guoxiu Wang*[a]

An *in situ* hydrothermal synthesis approach has been developed to prepare SnO_2@graphene nanocomposites. The nanocomposites exhibited a high reversible sodium storage capacity of above 700 mA h g^{-1} and excellent cyclability for Na-ion batteries. In particular, they also demonstrated a good high rate capability for reversible sodium storage.

Na-ion batteries are considered to be an alternative to Li-ion batteries owing to the natural abundance of sodium.[1] They have emerged as an attractive electrochemical power source for large-scale electrical energy storage (EES).[2–5] The Na ion has a larger ionic radius than that of the Li ion, making it more difficult to identify suitable electrode materials for Na-ion batteries. Electrode materials with an open framework are required for facile Na ion insertion/extraction. Following this strategy, many breakthroughs in cathode materials have been achieved, such as layered transition metal oxides,[6–9] three-dimensional $Na_{0.44}MnO_2$ with an S-shaped tunnel,[10,11] and Prussian blue with a new framework.[12] However, the development of suitable anode materials for Na-ion batteries remains a considerable challenge. It was found that hard carbon is a suitable anode material for Na-ion batteries because it has large interlayer distance and disordered structure.[13] However, Dahn *et al.* reported that the Na-intercalated hard carbon (Na_xC) has high reactivity with the non-aqueous electrolyte,[14] raising new concerns about the stability of the electrolyte when used as a carbon based electrode. Alternative oxide anodes such as $Na_2Ti_3O_7$[15] and amorphous TiO_2-nanotubes[16] have been investigated, but they all show less than 300 mA h g^{-1} capacities, which is far from meeting the demand of high energy storage. Transition metal oxides also did not achieve satisfactory performance,[17] although they have demonstrated excellent electrochemical properties in Li-ion batteries. Recently, it was found that anodes based on Na alloying reaction can dramatically improve the capacity of sodium storage.[18,19] It was reported that an SnSb–C nanocomposite achieved 544 mA h g^{-1} capacity, good rate capacity and cyclability for Na-ion storage,[18] and pure micrometric antimony can sustain a capacity close to 600 mA h g^{-1} at a high rate in Na-ion batteries.[20]

SnO_2 can also react with Na based on a reversible Na alloying reaction and generate an Na–Sn alloy, which has potential as anode materials for Na-ion batteries. Based on the reaction $4SnO_2 + 31Na^+ + 31e^- \rightarrow Na_{15}Sn_4 + 8Na_2O$,[18] SnO_2 can deliver a theoretical sodium storage capacity of 1378 mA h g^{-1}. However, large volume variation occurs during the charge–discharge process, inducing rapid capacity loss. Embedding SnO_2 in carbon matrices can effectively cushion the volume expansion of the SnO_2 electrode. Among various carbon matrices, graphene has several advantages such as superior conductivity, large surface areas, and excellent mechanical strength. Therefore, SnO_2–graphene nanocomposites could be a high performance anode material for Na-ion batteries.

Herein, we report *in situ* hydrothermal synthesis of SnO_2@graphene nanocomposites, in which SnO_2 nanocrystals are uniformly anchored on graphene nanosheets. The as-prepared SnO_2@graphene nanocomposites demonstrated a high reversible capacity of over 700 mA h g^{-1} in Na-ion batteries and an excellent cyclability.

SnO_2@graphene nanocomposites were synthesised by an *in situ* hydrothermal method. For comparison, bare graphene and SnO_2 nanocrystals were also prepared. Graphene oxide nanosheets were used as the precursor to prepare SnO_2@graphene nanocomposites, which were synthesized from natural graphite powders by a modified Hummer's method.[21] The crystallographic phases of as-prepared materials were identified by XRD (as shown in Fig. 1a). The bare SnO_2 can be well indexed as a tetragonal symmetry unit cell (JCPDS: 71-0652), with the space group of $P4_2/mnm$. For SnO_2@graphene nanocomposites, the strong diffraction lines can be indexed to the tetragonal SnO_2 phase and the weak diffraction peaks correspond to graphene (002) and (100) crystal planes, which confirm the co-existence of SnO_2 nanocrystals and graphene nanosheets.

[a] *Centre for Clean Energy Technology, School of Chemistry and Forensic Science, Faculty of Science, University of Technology, Sydney, NSW 2007, Australia. E-mail: Guoxiu.Wang@uts.edu.au; Fax: +61-2-9514-1460; Tel: +61-2-9514-1741*
[b] *School of Materials Science and Engineering, Gyeongsang National University, Jinju, South Korea*

† Electronic supplementary information (ESI) available: Detailed experimental procedures; FESEM image, TG/DTA curves, charge–discharge profiles, rate performance of bare SnO_2 and graphene, *ex situ* SEM images. See DOI: 10.1039/c3cc40448j

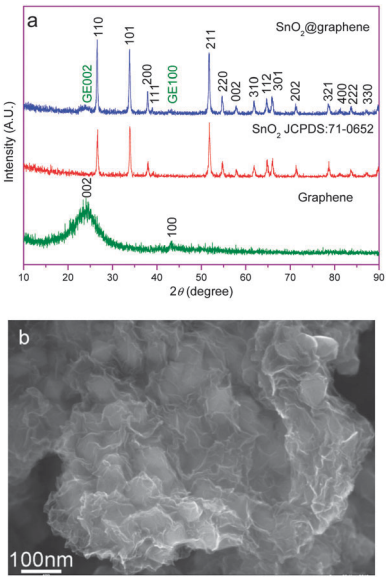

Fig. 1 (a) XRD patterns of bare graphene, bare SnO_2, and SnO_2@graphene nanocomposite. (b) FESEM image of SnO_2@graphene nanocomposites.

The morphology of SnO_2@graphene nanocomposites was characterised by FESEM. As shown in Fig. 1b, SnO_2 nanocrystals were homogeneously distributed on graphene nanosheets. It should be noted that individual SnO_2 nanocrystals are wrapped with graphene nanosheets. The sizes of SnO_2 nanocrystals are estimated to be about 60 nm. More FESEM images are shown in Fig. S1 (ESI†), which further depicts the morphological features of SnO_2@graphene nanocomposites.

The crystal structure and architecture of SnO_2@graphene nanocomposites were analysed by TEM and HRTEM analysis (as shown in Fig. 2). Fig. 2a shows a low magnification TEM image illustrating SnO_2 nanocrystals uniformly anchored on graphene nanosheets. When we analysed individual SnO_2 nanocrystals, we found that SnO_2 nanocrystals have a well-defined octahedral shape with an apex-to-apex length of around 60 nm (Fig. 2b). The inset (right bottom) in Fig. 2b illustrates their geometric model, which depicts their outline and projected direction. The selected area electron diffraction (SAED) of these nanocrystals is shown as an inset on the left-top corner in Fig. 2b, which can be well indexed along the [110] zone axis of tetragonal SnO_2. The spot SAED pattern array confirmed the single crystalline nature of SnO_2 nanocrystals. Fig. 2c shows another typical free-standing octahedral SnO_2 nanocrystal, which was observed from the top view. The corresponding FFT pattern along the [001] zone axis is shown as an inset in Fig. 2c (left bottom corner), which confirmed the growth of octahedral SnO_2 along the [001] direction. A lattice resolved HRTEM image is shown in Fig. 2d (recorded from the rectangular area marked in Fig. 2b). The regular arrangement of the (110) crystal planes is clearly visible. The orthogonal (001) and $(1\bar{1}0)$ crystal planes with 0.31 nm and 0.33 nm *d*-spacings, respectively, have been determined. The weight ratio between SnO_2 nanocrystals and graphene nanosheets was determined to be 60 : 40 by TG and DTA measurement (Fig. S2, ESI†). The 40 wt% weight loss occurred mainly from 400 to 500 °C with the feature of an endothermic peak at 447 °C, corresponding to the oxidation of carbon.

Applied as anode materials in Na-ion batteries, electrochemical performances of bare graphene, bare SnO_2, and SnO_2@graphene nanocomposites are shown in Fig. 3. They exhibit different discharge–charge profiles in the first and second cycles (Fig. 3a). For bare graphene nanosheets, the specific discharge capacity is 1009 mA h g^{-1} in the first cycle. It dramatically dropped to 237 mA h g^{-1} in the second cycle. Bare SnO_2 nanocrystals delivered 1773 and 473 mA h g^{-1} discharge capacities in the first and the second cycles, respectively, while SnO_2@graphene nanocomposites demonstrate the highest initial discharge capacity of 1942 mA h g^{-1}. After the first cycle, a capacity of 741 mA h g^{-1} was maintained. Similar to lithium

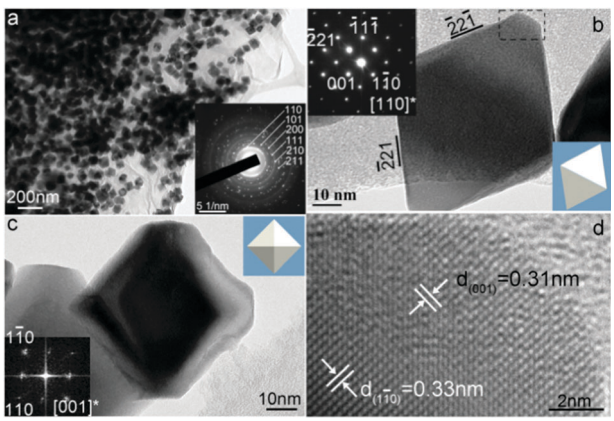

Fig. 2 (a) Low magnification TEM image of SnO_2@graphene nanocomposites. (b) and (c) are typical TEM images of single octahedral SnO_2 nanocrystals projecting from [110] and [001] directions, respectively. (d) is a lattice resolved HRTEM image taken from the rectangular area marked in (b). The inset in (a) is the SAED pattern. Right bottom inset in (b) and right top inset in (c) are the corresponding geometric models. The left top inset in (b) is the SAED pattern. The left bottom inset in (c) is the Fast-Fourier-Transform (FFT) pattern.

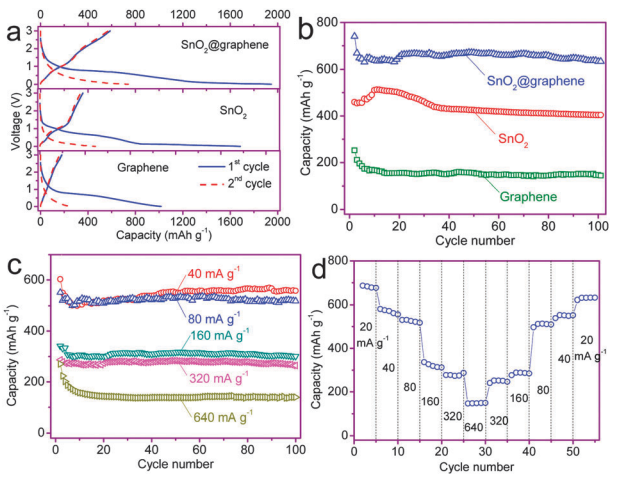

Fig. 3 (a) 1st and 2nd cycles discharge and charge profiles of bare graphene, bare SnO_2, and SnO_2@graphene nanocomposites at 20 mA g^{-1} current density. (b) Cycling performance of bare graphene, bare SnO_2, and SnO_2@graphene nanocomposites at 20 mA g^{-1} current density. (c) Cycling performance of SnO_2@graphene nanocomposites at current densities of 40, 80, 160, 320, and 640 mA g^{-1}. (d) Rate performance of SnO_2@graphene nanocomposites at varied current densities. (b–d) are recorded from the 2nd cycle.

ion batteries, the irreversible capacity in the first cycle could be consumed to form the solid electrolyte interface (SEI) layer on the surface of the electrode. From the second cycle, Na storage capacities of all tested electrodes had stabilised (as shown in Fig. 3b). SnO_2@-graphene nanocomposites delivered an average of more than 700 mA h g^{-1} capacity in 100 cycles. The value is much higher than that of bare SnO_2 nanocrystals and bare graphene nanosheets. In particular, SnO_2@graphene nanocomposites demonstrated an excellent capacity retention capability with almost no capacity fading within 100 cycles. This was evidenced in Na storage capacity reaching 638 mA h g^{-1} after 100 cycles for the SnO_2@graphene nanocomposite anode. The discharge–charge profiles of SnO_2@graphene nanocomposites in the 5th, 20th and 100th cycles tested at 40 mA g^{-1} current density are shown in Fig. S3 (ESI†). The overlapped curves indicate the stable nature and excellent cyclability of the electrode.

Fig. 3c shows the cycling performance of SnO_2@graphene nanocomposite electrodes at different current densities (from the second cycle). The nanocomposite exhibited decent high rate performance. After 100 cycles, the discharge capacities were maintained at high values when cycled at different current densities: 569 mA h g^{-1} at 40 mA g^{-1}, 508 mA h g^{-1} at 80 mA g^{-1}, 302 mA h g^{-1} at 160 mA g^{-1} and 263 mA h g^{-1} at 320 mA g^{-1}. Even when cycled at 640 mA g^{-1}, a discharge capacity of 143 mA h g^{-1} was still obtained after 100 cycles. The high rate performance of SnO_2@graphene nanocomposites is much better than that of bare SnO_2 and graphene electrodes (Fig. S4, ESI†) and previously reported anode materials for Na-ion batteries.[15,16,22,23] We also tested the cycling performance of SnO_2@graphene nanocomposites at varied current densities (Fig. 3d). After cycling at high current densities, the cell capacity can recover to the original values as long as the current density reversed back to low current density. This confirmed that SnO_2@graphene nanocomposites are tolerant to high rate cycling.

The outstanding performance of SnO_2@graphene nanocomposites could be ascribed to the unique 3D architecture of the material. During the discharge and charge process, Na ions reversibly react with SnO_2 to form Na_xSn and Na_2O:[18,19,24–26]

$$(4 + x)Na^+ + SnO_2 + (4 + x)e^- \leftrightarrow Na_xSn + 2Na_2O \quad (1)$$

This process usually accompanies large volume change. As illustrated by FESEM and TEM characterisation, individual SnO_2 nanocrystals are embedded and wrapped by flexible and conductive graphene nanosheets. The cycled SnO_2–graphene electrodes were further examined by *ex situ* SEM as shown in Fig. S5 (ESI†). We can observe that graphene nanosheets still preserved their original morphology and SnO_2 nanoparticles lost their octahedral shape and disintegrated into less than 5 nm nanoparticles (Fig. S5c, ESI†) due to the reaction with Na ions after 100 cycles. Furthermore, it should be noted that SnO_2 nanoparticles are uniformly distributed in the graphene matrix. On the contrary, the bare SnO_2 nanoparticles show cracking and crumbling of the structure after 100 cycles (Fig. S6, ESI†). The graphene matrix can effectively buffer the volume variation during the Na insertion and extraction process. Furthermore, graphene nanosheets also serve as conductive media for electron transfer during the discharge and charge process. As a result, the integrity of the electrode can be maintained, leading to an enhanced performance for Na storage.

In conclusion, SnO_2@graphene nanocomposites with 3D architecture were synthesized by an *in situ* hydrothermal method. Homogeneous distribution of SnO_2 nanocrystals on graphene nanosheets has been confirmed by FESEM and TEM characterisation. HRTEM analysis identified that SnO_2 nanocrystals (~60 nm in size) have an octahedral shape. Galvanostatic charge–discharge measurements show the highly reactive nature of SnO_2@graphene nanocomposites towards sodium storage in Na-ion cells. The nanocomposites demonstrated a high reversible specific capacity of above 700 mA h g^{-1}, excellent cyclability, and decent high rate performance, which could be ascribed to the unique 3D architecture of the nanocomposites. SnO_2@graphene nanocomposites could be a promising high performance anode material for Na-ion batteries.

This work was financially supported by the Australian Research Council (ARC) through the ARC FT project (FT110100800). We also acknowledge the support from the National Research Foundation of Korea through the WCU (R32-20093) project.

Notes and references

1 V. Palomares, P. Serras, I. Villaluenga, K. B. Hueso, J. Carretero-Gonzalez and T. Rojo, *Energy Environ. Sci.*, 2012, **5**, 5884.
2 A. Ponrouch, E. Marchante, M. Courty, J.-M. Tarascon and M. R. Palacin, *Energy Environ. Sci.*, 2012, **5**, 8572.
3 J. B. Goodenough, *J. Solid State Electrochem.*, 2012, **16**, 2019.
4 B. L. Ellis and L. F. Nazar, *Curr. Opin. Solid State Mater. Sci.*, 2012, **16**, 168.
5 P. Barpanda, S.-I. Nishimura and A. Yamada, *Adv. Energy Mater.*, 2012, **2**, 841.
6 R. Berthelot, D. Carlier and C. Delmas, *Nat. Mater.*, 2011, **10**, 74.
7 D. Kim, E. Lee, M. Slater, W. Q. Lu, S. Rood and C. S. Johnson, *Electrochem. Commun.*, 2012, **18**, 66.
8 X. Xia and J. R. Dahn, *Electrochem. Solid-State Lett.*, 2012, **15**, A1.
9 N. Yabuuchi, M. Kajiyama, J. Iwatate, H. Nishikawa, S. Hitomi, R. Okuyama, R. Usui, Y. Yamada and S. Komaba, *Nat. Mater.*, 2012, **11**, 512.
10 Y. L. Cao, L. F. Xiao, W. Wang, D. W. Choi, Z. M. Nie, J. G. Yu, L. V. Saraf, Z. G. Yang and J. Liu, *Adv. Mater.*, 2011, **23**, 3155.
11 F. Sauvage, L. Laffont, J. M. Tarascon and E. Baudrin, *Inorg. Chem.*, 2007, **46**, 3289.
12 Y. Lu, L. Wang, J. Cheng and J. B. Goodenough, *Chem. Commun.*, 2012, **48**, 6544.
13 Y. L. Cao, L. F. Xiao, M. L. Sushko, W. Wang, B. Schwenzer, J. Xiao, Z. M. Nie, L. V. Saraf, Z. G. Yang and J. Liu, *Nano Lett.*, 2012, **12**, 3783.
14 X. Xia, M. N. Obrovac and J. R. Dahn, *Electrochem. Solid-State Lett.*, 2011, **14**, A130.
15 P. Senguttuvan, G. Rousse, V. Seznec, J.-M. Tarascon and M. R. Palacin, *Chem. Mater.*, 2011, **23**, 4109.
16 H. Xiong, M. D. Slater, M. Balasubramanian, C. S. Johnson and T. Rajh, *J. Phys. Chem. Lett.*, 2011, **2**, 2560.
17 S. Komaba, T. Mikumo, N. Yabuuchi, A. Ogata, H. Yoshida and Y. Yamada, *J. Electrochem. Soc.*, 2010, **157**, A60.
18 L. F. Xiao, Y. L. Cao, J. Xiao, W. Wang, L. Kovarik, Z. M. Nie and J. Liu, *Chem. Commun.*, 2012, **48**, 3321.
19 Y. Xu, Y. Zhu, Y. Liu and C. Wang, *Adv. Energy Mater.*, 2013, **3**, 128.
20 A. Darwiche, C. Marino, M. T. Sougrati, B. Fraisse, L. Stievano and L. Monconduit, *J. Am. Chem. Soc.*, 2012, **134**, 20805.
21 W. S. Hummers and R. E. Offeman, *J. Am. Chem. Soc.*, 1958, **80**, 1339.
22 R. Alcantara, P. Lavela, G. F. Ortiz and J. L. Tirado, *Electrochem. Solid-State Lett.*, 2005, **8**, A222.
23 D. A. Stevens and J. R. Dahn, *J. Electrochem. Soc.*, 2000, **147**, 1271.
24 J. W. Wang, X. H. Liu, S. X. Mao and J. Y. Huang, *Nano Lett.*, 2012, **12**, 5897.
25 L. D. Ellis, T. D. Hatchard and M. N. Obrovac, *J. Electrochem. Soc.*, 2012, **159**, A1801.
26 M. K. Datta, R. Epur, P. Saha, K. Kadakia, S. K. Park and P. N. Kumta, *J. Power Sources*, 2013, **225**, 316.